EFDA–JET–PR(13)53

T. Craciunescu, A. Murari, M. Gelfusa, I. Tiseanu, V. Zoita
and JET EFDA contributors

# Overview of Image Processing Tools to Extract Physical Information from JET Videos

# Overview of Image Processing Tools to Extract Physical Information from JET Videos

T. Craciunescu[1], A. Murari[2], M. Gelfusa[3], I. Tiseanu[1], V. Zoita[1,4]
and JET EFDA contributors*

***JET-EFDA, Culham Science Centre, OX14 3DB, Abingdon, UK***

*[1]EURATOM-MEdC Association, NILPRP, Bucharest, Romania*
*[2]Consorzio RFX, Associazione EURATOM-ENEA per la Fusione, Padova, Italy*
*[3]Associazione EURATOM-ENEA - University of Rome "Tor Vergata", Roma, Italy*
*[4]EFDA-JET CSU, Culham Science Centre, OX14 3DB, Abingdon, OXON, UK*
** See annex of F. Romanelli et al, "Overview of JET Results",*
*(24th IAEA Fusion Energy Conference, San Diego, USA (2012)).*

Preprint of Paper to be submitted for publication in Proceedings of the
8th Workshop on Fusion Data Processing, Validation and Analysis, Ghent, Belgium
4th November - 6th November 2013

**ABSTRACT**

In Magnetic Confinement Nuclear Fusion devices such as JET, the last years have witnessed a significant increase of the use of digital imagery, not only for the surveying and control of the experiments, but also for the physical interpretation of results. More than 25 cameras are routinely used for imaging on JET in the IR and visible spectral regions. These cameras can produce up to tens of Gbytes per shot and their information content can be very different, depending on the experimental conditions. However, the relevant information about the underlying physical processes is generally of much reduced dimensionality compared to the recorded data. The extraction of this information, which allows full exploitation of these diagnostics, is a challenging task. The image analysis consists, in most cases, of inverse problems which are typically mathematically ill posed. The typology of objects to be analysed is very wide and usually the images are affected by noise, saturation, low grey-level in-depth resolution, reshaping of moving objects, etc. Moreover, the plasma events have time constants of ms or tens of ms, which imposes tough conditions for real-time applications. On JET, in the last few years, new tools and methods have been developed for physical information retrieval. The methodology of optical flow has allowed, under certain assumptions, deriving information about the dynamic of video objects, associated with different physical phenomena such as instabilities, pellets, and filaments. The approach has been extended in order to approximate the optical flow within the MPEG compressed domain, allowing the manipulation of the large JET video databases and, in specific cases, even real-time data processing. The fast visible camera may provide new information potentially useful for disruption prediction. A set of methods, based on the extraction of structural information from the visual scene, have been developed for the automatic detection of MARFE (*Multifaceted Asymmetric Radiation From the Edge*) occurrence, which precede disruptions in density limit discharges. An original spot detection method has been developed for large surveys of videos in JET and for the assessment of the long term trends in their evolution. The analysis of JET IR videos, recorded during JET operation with the ILW (*ITER–Like Wall*), allows the retrieval of correlation of the evolution of spots properties with macroscopic events, in particular series of intentional disruptions.

## 1. INTRODUCTION

Visual information has always played an important role during the evolution of science. Starting from manual drawings documenting the experiments, imaging increased its role with the invention of photography and its prominent use in astronomy and particle physics. The last years have witnessed a huge development and widespread use of video and computer technology. Digital video cameras have become a tool of convenience, being used in a variety of devices to record information. Multimedia software and hardware are nowadays standard tools for handling images and videos, allowing information sharing, with a clear impact on society. Science follows naturally this evolution, image processing becoming a standard scientific tool for various scientific applications and large experiments. In particular, digital video cameras have become very popular in magnetic confinement nuclear fusion devices such as JET. More than 25 cameras are routine used for imaging

in JET, in the IR and visible wavelength regions, for various purposes, from surveying and control to scientific investigations. The applications range from the protection of the new JET ITER-like Wall (ILW) to detailed investigations of the plasma wall interactions and of various instabilities.

The active protection of the plasma facing components is essential in order to manage high power and particle loads of high temperature plasmas. This problem is a major issue since the installation in JET of the ITER-Like Wall (ILW) [1] which comprises solid beryllium limiters and a combination of bulk W and W-coated CFC divertor tiles but with no active cooling. Image processing can play an important role if the analysis is provided in real time and therefore a significant technological and scientific effort has been devoted to this subject. A new endoscope with optimised divertor view has been developed in order to survey and monitor the emission of specific impurities [2]. A new wide angle view camera system, which considerably increases the coverage of the vessel, was recently installed [3]. New infrared diagnostics imaging the horizontal and vertical tiles of the divertor were also installed [4]. Different kinds of modelling have been applied for assessing the consistency of the information provided by the IR cameras with other diagnostics for temperature control [5]. These diagnostics proved to provide valuable information for disruption heat loads studies [6-7]. A different approach, which relies on the computational paradigm of cellular nonlinear networks and on the use of field-programmable gate arrays (FPGA),has been developed for the detection of hot-spots in the vacuum vessel [8].

The amount of data produced by the routine operation of video cameras is a critical issue. Some of these cameras are very fast and can produce even two Gbytes of data per shot, leading to the gradual accumulation of enormous databases. Automatic tools are strictly necessary for handling the large amount of video information. The original data (too voluminous to understand) should be mapped into a more compact and abstract form in order to allow the extraction of the relevant information about the underlying physical processes and their interpretation. In order to retrieve this information, the image processing methods have to deal with images frequently affected by noise, saturation, low grey-level in-depth resolution, reshaping of moving objects, etc. and containing a wide typological variety of video objects. Under these difficult experimental constraints, the image analysis consists usually of inverse problems which are typically mathematically ill posed. The retrieval of the useful information in real time represents also a major challenge, as the plasma events have time constants of ms or tens of ms.

A package of tools has been developed for the intelligent and automatic handling of the continuously growing database. Content-based image retrieval methods [9-10] have been developed based on data screening of morphological aspect of images. Assuming that diagnostics generate reproducible patterns for similar physical behaviour, these tools ensure an efficient high level data access to the huge JET image database. Beside the searching instruments, the classification tools are indispensable for database manipulation. Machine learning techniques have been implemented for constructing the taxonomy of the various objects appearing in the frames recorded by the visible cameras [11].

Image processing methods for physical information retrieval, analysis and interpretation have

been developed in the last few years. These methods are reviewed in this paper which is organized in three main sections. The first is dedicated to tools for deriving information about the velocity of video objects (generated by instabilities, pellets, etc) and for exploring dynamic processes. The next section is dedicated to a set of methods which exploit the structural information contained in the visual scene in order to identify plasma events. They are potentially useful for disruption prediction in case of a future upgrade of the hardware of the cameras allowing real time data streaming. The long term trends and evolution of the dust particles, which have fallen onto the divertor surfaces and the correlation with macroscopic events by image processing, are the subject of the last section. Several conclusions are drawn in the last section of the paper.

## 2. IMAGE PROCESSING FOR EXPLORING DYNAMIC PROCESSES

The estimation of motion information from image sequences is a recurrent problem in computer vision. In fusion, the poor accessibility of the devices makes very difficult the deployment of more than one camera with the same field of view. Therefore stereoscopic methods are rarely applicable. An alternative to retrieve information about the velocity of moving objects, which leaves a signature on the video frames, is the optical flow concept. The optical flow is defined as the "flow" of grey values at the image plane and it is an approximation of the motion field, i.e. of the real motion of the object in the 3-Dscene, projected onto the image plane. The quality of this approximation depends on how much the objects change the irradiance on the image plane while moving in the scene.

Most of the existing algorithm starts from the brightness constancy assumption which assumes that all changes in the image are caused by the translation of brightness patterns leading to the gradient constraint equation:

$$\vec{f}_S \cdot \vec{v} + \vec{f}_S = 0 \qquad (1)$$

Where and are the spatial and temporal gradients and is the optical flow velocity. In this way it is assumed implicitly also that the illumination in the scene is uniform and surfaces appear equally bright from all viewing directions. Also the image formation process in the camera is supposed to be free of distorting effects.

From the mathematical point of view the problem of finding the flow field solution of equation (1) is an ill-posed one. The brightness constancy assumption provides just one constraint on the two unknowns at each pixel. Moreover, the so-called aperture problem brings additional uncertainty in the determination of the optical flow. Spatial and temporal grey value changes can be derived with local operators which compute the corresponding local derivatives using masks. The masks restrict the operator's access to a local region of the observed object, equal to the size of mask. Consequently, finding unequivocal corresponding points in two consecutive images of a sequence become problematic. For example, an unambiguous determination of the displacement is possible only if a corner of the object is within the mask [12]. Therefore, supplementary constraints must be introduced in order to alleviate these difficulties. The most widely used techniques rely on a global

strategy, attempting to minimize a global energy functional [13] or on the optimization of some local energy-like expression [14]. Global and local methods have complementary advantages and shortcomings.

A common approach for the global methods is the introduction of an additional term in Eq. 1 that assumes a smooth variation of the flow across the image. Then, the optical flow can be retrieved as the minimizer of the following global energy functional:

$$E_{global}(u, v) = [(f_x u + f_y v + f_t)^2 + \alpha (|\nabla u|^2 + |\nabla v|^2)]\, dxdy \tag{2}$$

where is a regularising parameter which determines the smoothness of the flow field, and are the and components of the flow, respectively. By mean of the smoothness term, this approach has the advantage of producing dense flow fields (one motion vector per pixel). Unfortunately the global methods have been observed to be sensitive to noise and outliers. Additional smoothing of input images has been used to reduce the effect of noise and to stabilize the differentiation process. Smoothing has been extended also to the temporal dimension. Various related penalty functions, together with different optimization algorithms and implementations, have been also defined in order to tackle this problem (see Ref. [15] for a review).

Local methods assume a small neighbourhood of constant flow. For a neighbourhood of size, the optic flow can be determined at the location from a weighted least square fit by minimizing the function:

$$E_{local}(u, v) = K_\rho \times (f_x u + f_y v + f_t)^2 \tag{3}$$

A certain amount of smoothing, introduced by the Gaussian smoothing operator is very successful in rendering the method robust against noise. Unfortunately this feature is counterbalanced by the behaviour in the flat regions of the image, where the gradient vanishes and the method become unable to produce dense flow fields.

Bruhn et al. [16] exploited the similarity between the formulation (3) of the local methods and the first term under the integral in the formulation (2) of the global approach, in order to formulate a hybrid combined local-global (CLG) class of methods. The following notation is normally adopted to discuss these techniques:

$$\nabla_3 f \equiv (f_x, f_y, f_t)^T \qquad J_p(\nabla_3 f) \equiv K_\rho * (\nabla_3 f, \nabla_3 f^{\mathrm{T}})$$

$$w \equiv (u, v, 1)^T \qquad |\nabla w|^2 \equiv |\nabla u|^2 + (|\nabla v|^2$$

The equations (2) and (3) can be rewritten in a way which makes obvious the similarity between the two paradigms:

$$E_{global}(w) = f_\Omega [(w^T J_0(\nabla_3 f)\, w + \alpha |\nabla w|^2]\, dxdy \tag{4}$$

$$E_{local}(w) = w^T J_p(\nabla_3 f)\, w \tag{5}$$

The CLG method is obtained by replacing in (4) the matrix with the structure tensor , for some integration scale . This approach brings together the ability of the global methods to produce dense flow fields and the robustness against noise of the local methods. This class of methods has been studied and optimized for the very specific case of JET images [17].

The optical flow methodology has been applied for the videos provided by the wide angle view fast visible camera (Photron APX) [18] which is installed on the wide angle endoscope [19]. The camera is viewing the full poloidal cross-section of the vacuum vessel and is covering a toroidal extent of $90^o$ (Fig.1). It has a 1024x1024 CMOS pixel detector, allowing image acquisition with a frame rate up to 3kHz. The maximum frame rate of the camera is 250 kframes/s (for a reduced frame of 128×16 pixels).

The images used as input for the optical flow calculation are frequently affected by noise, saturation, low grey-level in-depth resolution, discontinuous movement, reshaping of moving objects. Therefore the basic assumptions of the optical flow model may not be always satisfied. Dedicated techniques able to prevent an inaccurate velocity computation have been devised. Particularly important is to deal with large displacements of objects between consecutive frames. A multi-resolution coarse-to-fine procedure [20] has been implemented. Occlusions, which appear when two objects that are spatially separated in the 3D space might interfere with each other in the projected 2D image plane, are treated by comparing the forward and reverse flow fields and labeling pixels as occluded where the two disagree [21]. In a number of cases, high-order filter constancy has been used to reduce the influence of lighting changes [22]. A procedure for the assessment of the uncertainties of the method has been also developed and applied. The similarity between a certain image in the video stream and its reconstruction using the previous image and the optical flow is used as confidence criterion (see Ref. 17 for details). After implementing these procedures the optical flow method has been successfully used for the evaluation of the speed of various plasma instabilities, in particular ELM filaments and MARFEs.

The propagation of the filamentary coherent structures observed during the development of ELM instabilities is important to the overall dynamics in a variety of plasmas. Their interaction with the tokamak first wall (divertor and limiter tiles) is one of the critical issues for ITER due to the deposited heat loads [23]. The filament temperature and composition may differ from the background plasma, determining and enhanced visible radiation. The speed of filaments can be estimated when they can be tracked along the surface of the outer limiters. The known geometrical dimension of the limiters allows the conversion of image pixels in length units and consequently the determination of speed in absolute units. The motion segmentation can be obtained by thresholding the optical flow modulus image and applying morphological operators (dilation, erosion). A typical example is presented in Fig.2.

The MARFE instability is a tokamak edge phenomenon characterized by greatly increased radiation, density fluctuations, and decreased temperature in a relatively small volume [24]. MARFE

are the manifestation of a thermal instability, with impurity radiation being the main energy loss mechanism from their volume. They determine a significant increase in impurity radiation, leaving a clear signature in the videos recorded by the fast visible camera in JET with the carbon wall (Fig. 3). MARFEs moves up and down the vacuum vessel on the high field side. The known structures of the tokamak vacuum vessel allow the inference of the velocity in the real space from the 2D image analysis. An illustrative example is presented in Fig.3

The optical flow method proved to be a useful tool also for obtaining various kind of information related to pellets. Cryogenic pellet injection is one of the prime candidates to fuel large scale fusion devices, including ITER and DEMO, in different operational regimes, including the standard H-mode foreseen as ITER`s baseline scenario. Pellet fuelling has been demonstrated to open access to operational regimes not reachable by gas puffing [25]. The pellets represent also a tool for controlling the edge localized modes (ELMs), especially for the mitigation of type-I ELMs in large fusion experiments [26-27].

The methodology developed in JET has been used in recent investigations on ASDEX-UG, for the predictive understanding of the underlying processes of the pellet-plasma interaction [28]. Using a fast framing camera system (600kHz frame rate) [29] it was possible to ensure appropriate spatial and temporal resolution for the investigation of pellet ablation dynamics, a complex 3D process taking place on the μs timescale. The optical flow has provided information for the analysis of pellet cloud dynamics and drifts and particularly for the study of the process of eruption of secondary cloudlets located around the main cloud pellet.

A controlled high pellet fuelling efficiency is needed as otherwise the beneficial effects are spoiled by the increase of neutral pressure from fuel losses. The optical flow proved to be useful in assessing the preparation of the pellets, for evaluating the ice extrusion velocity which is one of the parameters that influence the efficiency of the pellet injection on ELM triggering. The High Frequency Pellet Injector, part of the JET programme in support of ITER [30], is equipped with a set of diagnostics aiming at helping in the injector operation and at measuring the injection parameters. Among them, a CCD camera monitors the quality and the dimensions of the extruded ice and it can be used also for the determination of the extrusion speed. Typical images provided by this camera are presented in Fig. 4, together with the evaluation of the optical flow [31]. However, for a routine examination of the extrusion process, the optical flow calculation time must be compatible with the online constraints imposed by the image acquisition frame rate (50Hz). A significant reduction of the computation time be could be obtained if a region of interest the optical flow calculation is performed only inside a certain region of interest (ROI). But, as the ribbons of ice are floating in the image (see Fig.5), a procedure for splitting the video scene into multiple motion/static regions must be implemented, allowing the dynamical estimation of the ROI.

A solution resides in using the information provided by the way in which the videos are stored, in a compressed format, for further analysis. For example, the MPEG format [32] comprises a crude estimation of the motion field which is evaluated for compression purposes. MPEG exploits the statistical redundancies in both temporal and spatial directions. The spatial redundancy is

reduced by means of the discrete cosine transform. As the transform concentrates the energy into the low-frequency coefficients, the bit rate reduction is obtained by the coarse quantization of the high-frequency coefficients. But the high degree of compression specific to MPEG is achieved in the temporal dimension, assuming a simple translation motion between consecutive frames. The magnitude of a particular image pixel can be predicted from pixels of a nearby frame using a block matching method. The parts of the image that do not change significantly are simply copied from other areas or other frames. In case of the other parts, the algorithm searches for the best matching block. A set of motion vectors are implicitly defined by the different position of the matching blocks in the actual and reference frame, respectively. As a compromise must be found between the accuracy in predicting complex motion in the image and the expense of transmitting the motion vectors, only one motion vector is estimated for an image block of 16×16 pixels, limiting the resolution of the motion segmentation. However this resolution is sufficient for the dynamic segmentation of the ROI for ice extrusion velocity evaluation. Additional procedures are needed in order to obtain a reliable procedure, appropriate for the routine analysis of large sets of data. Sometimes the motion vectors information is heavily corrupted by the sudden occurrence of lack of correlation between estimated motion vectors and real motion in the video scene. The motion vectors can be transformed into a smoother motion field using a set of regularization set of rules [33] and a confidence measure [34] to ensure that the motion field is meaningful. The removal of isolated vectors that have a low probability of reflecting a certain real movement in the image is obtained assuming that a moving object can be assimilated with a group of pixels in which the motion vectors are consistent with each other. Pixel grouping can be obtained using a block growing procedure which uses as starting point a seed pixel corresponding to the local maximum grey-level and its 4-connected neighbours. The region grows by adding each ungrouped bordering pixel if a consistency criterion, based on the grey-level difference, is satisfied [35]. A typical motion segmentation result, using the motion estimation within the MPEG video compressed domain, is presented in Fig.5. The computation time needed for the dynamically determination of the ROI is ~1.5ms and the total optical flow calculation is less than 20ms, allowing, in principle, the online evaluation of the optical flow [36]. Another advantage of the approach consists of the possibility of engrafting the optical flow algorithm in the MPEG compressing routine.

## 3. IMAGE PROCESSING FOR PLASMA PHYSICAL EVENTS DETECTION

The fast visible camera may provide useful information also for the detection of anomalous behaviour in the discharges with potential harmful consequences. MARFEs and UFOs (*Unidentified Flying Objects*) leave distinct signatures in the video data opening the possibility of automatic detection of these events. MARFEs normally precede density limit disruptions. Therefore the detection of MARFEs may be used for automatic disruption prediction. The automatic detection of UFOs, which are flakes released by JET first wall as a consequence of unusual power loads, typically due to instabilities like ELMs, may be an important tool for machine protection and disruption avoidance. As already mentioned and illustrated in Fig. 3, MARFEs leave a distinctive signature in the video

data, appearing like ribbon-like shapes moving up and down the vacuum vessel on the high field side. This specific shape can be exploited for automatic identification. However the identification should avoid confusion with other video objects with similar shapes, like e.g. flashes, probably caused by ELMs (Edge Localized Modes) or high radiation from the poloidal limiters.

A set of methods, based on the extraction of structural information from the visual scene, have been developed. They can be used for content-based retrieval of relevant frames from the large JET database but using MARFE detection for signalling disruptions; their deployment in real time, represent also an appealing application. In JET, with a carbon wall, the time elapsing between the occurrence of a MARFE and the following disruption (in density limit discharges) is of the order of several hundreds of milliseconds, allowing enough time for calculations and for the following action of the mitigation tools. At his point it has to be mentioned that currently, on JET, the fast imaging systems are not yet used for their real-time control. The real-time identification of MARFEs, using some of the methods described in this section, will require an upgrade of the hardware of the cameras since the ones presently used cannot perform real time streaming of the videos.

The first approach for automatic MARFE identification has been proposed in Ref. 37.The first step consists in isolating the objects occurring in the image by background subtraction. A method allowing a fast adaptation to changes of the scene has been implemented. The segmentation is a combination of image differencing with respect to a median background and a Laplacean operator [38]. An alternative consists of using the MPEG motion field combined with simple morphological operators (dilation, erosion, median filtering) [36]. Illustrative examples are presented in Fig. 6. The identification of moving objects is followed by a pattern recognition step which must discriminate between MARFEs and other video objects produced by different physical phenomena. The geometrical properties of the objects can be determined by means of statistical Hu moments [39], which are a combination of central moments of an object in an image. The advantage consists on obtaining information invariant to translation, rotation and scaling. During object tracking several metrics are evaluated in order to estimate the motion characteristics. A Support Vector Machines (SVM) classifier has been trained for automatic identification.

Recently, a highly parallelized software implementation of this method has been reported [40]. The algorithm is built in serial and parallel versions and written in C/C++ using OpenCV, cvBlob and LibSVM libraries. The main parallelization has been achieved separating image segmentation and pattern recognition. Several data parallelism and pipeline strategies have been also implemented inside these two groups. An image processing rate of more than 10,000 frames/s has been achieved on a dedicated Intel Symmetric MultiProcessing (SMP) computer architecture with a Linux™ operating system. In the same time a correct classification rate of 97.6% has been achieved.

A different way to extract structural information from the visual scene is based on the phase congruency (PhC) theory. PhC is a biological inspired tool for image processing which assumes that the human visual system understands the image mainly based on its low-level features (especially edges and zero-crossing). Biological and psychological processes aggregate in specific tools allowing the extraction of the highly informative structural features from the very redundant

imagistic information. Morrone et al. [41] assumes that visually discernible features coincide with those points where the Fourier waves, at different frequencies, have congruent phases. These points are characterized by a maximal local energy:

$$E(x) = \sqrt{F(x)^2 + H(x)^2} \tag{6}$$

where and are the responses of symmetric/anti-symmetric matched filters, of identical amplitude spectrum but differing in phase spectrum by 90 degrees. PhC is equal to the energy scaled by the sum of the Fourier amplitudes:

$$PhC(x) = w(x)^2 \cdot \frac{E(x) = T}{\Sigma_n A_n(x) + \varepsilon} \tag{7}$$

where represents the amplitude of the *n*-th Fourier component. The constants and are introduced in order to deal with the case when all the Fourier amplitudes are very small and to eliminate spurious responses to noise, respectively. PhC is significant only if it occurs over a wide range of frequencies, for a specific location. Therefore the weighting factor is introduced in order to penalize PhC at locations where the spread of the filter responses is narrow (see Ref. 42 for details).
Appropriate choices for the symmetric/anti-symmetric pairs of filters in case of 2D images are the Gabor filters [43]. They are also bio-inspired tool for image processing. Daugman [44] showed that the receptive field of most orientation receptive neurons in the (cat's) brain is similar to Gabor functions. These filters are constructed using a Gaussian kernel function modulated by a sinusoidal plane wave. In this way the filter responds to a specific frequency in localized region of the image. A lateral extension of the filters is introduced by means of a spreading function (usually Gaussian) applied across the filter, perpendicular to its orientation. PhC can be calculated over several orientations, in order to detect features with different anisotropic characteristics and the results are combined by summing and normalisation. It has the advantage of being a dimensionless quantity, providing information that is invariant to image illumination, contrast, and magnification.

For MARFE detection, PhC is evaluated for each frame in the video sequence and also for a number of reference frames displaying typical MARFE shapes. The structural similarity between the current and the reference frames is evaluated by calculating the similarity map [45]:

$$SIM(x) = \frac{2 \cdot PhC^{cur} \cdot PhC^{ref} + T'}{(PhC^{cur})^2 + (PhC^{ref})^2 + T'} \tag{8}$$

where and are calculated for the current frame and for the reference frame, respectively and is a positive constant introduced in order to ensure the stability of the calculation. For multiple reference images the corresponding similarity indexes are multiplied in order to obtain a global structural similarity map. The map, which contains similarity values calculated at each location , can be pooled into a single similarity score by summing the values for locations:

$$SIM_{score} = \frac{1}{D} \int_{\chi \in \Omega} SIM(x) dx \tag{9}$$

where is the map domain and is its area. MARFEs can be identified by mean of the detection of the peaks in the evolution of whose height is above a certain threshold. The same threshold value has been used for the whole JET MARFE video database. The PhC classifier ensures a good prediction rate: 96.2% events have been are correctly interpreted while from the misclassified events 0.03% are false positives and 3.5% false negatives [46]. An illustrative example is presented in Fig. 7, where the evolution of the is presented for JET Pulse No: 50053.

Another alternative way to automatically capture the essence of the MARFE visual patterns relies on sparse image representation (SIR), which consists of modelling images as a linear combination of a few elements from a dictionary is the total number of pixels in the image and is the total number of atoms in the dictionary). An efficient transform-based representation requires sparsity, that is, a large amount of information has to be compressed and expressed by a reduced set of transform coefficients. Recent results support the idea that learned dictionaries significantly outperforms off-the-shelf ones [47-48]. Therefore the dictionary and the image representation are learned simultaneously by solving the optimization problem:

$$\{\alpha, D, f\} = argmin_{\alpha, D, g}\left\{ \underbrace{\Sigma_{j=1}^{M}\|g_j - D\alpha_j\|_2}_{\substack{image \\ reconstruction}} + \underbrace{\lambda\Sigma_{l=1}^{L}\|\alpha_l\|_0}_{sparsity} \right\} \tag{10}$$

where are overlapping patches extracted from the image and $M$ is the total number of patches. The use of patches makes the problem tractable for large images; is a regularization parameter which balances between the two terms of the objective function. The first term attempts to minimize the image reconstruction error while the second one works for obtaining a representation as sparse as possible. The high dimensionality optimization problem can be efficiently manipulated using the K-SVD iterative method [49]. K-SVD is a generalization of the K-means clustering process that alternates between sparse coding of the images based on the current dictionary and a process of updating the dictionary elements to fit better the data. The sparse coding is implemented using an orthogonal matching pursuit (OMP) algorithm [50] which first find the dictionary element that has the biggest inner product with the image patches, and then subtract the contribution due to that element, and repeat the process until the image is satisfactorily decomposed.

For MARFE classification, a supervised learning strategy has been implemented. The dictionary has been learned adaptively from the training data (a set of images containing MARFEs) using the procedure described above. At this step the sparsity condition has not been applied allowing an arbitrary number of atoms to represent each image, until a specific representation error, related to the estimated image noise, is reached. The dictionary retrieved using this procedure contains enough information for the reconstruction of images belonging to the same class with the images in the training set. The representations are relatively robust against distortions and missing data. However, for images containing patterns with different characteristics, the reconstruction error increase significantly and this behaviour can be used to discriminate between classes of images. The dictionary is used to derive a representation for each image of the video sequence, limiting

the number of terms in the representation (the sparsity condition is now applied). Then a similarity map between the image and its representation can be calculated using a relation similar to Eq. (8). Again, the similarity map, which contains values calculated in each image pixel, can be pooled into a single score by a summation over the image. MARFE events can be identified as peaks with FWHM (full width at half maximum) below a certain threshold. The same threshold value has been used for the whole JET MARFE video database. The use of redundant representations and sparsity as driving forces for MARFE identification has allowed to correctly classifying 94.8% of the MARFE events. Among the misclassified events, a rate of 4.4% corresponds to false positive events and 0.8% to false negatives. A representative result is illustrated in Fig.7. The complete details of the implementation are reported in Ref. 51.

Local object shapes can be efficiently identified by the distribution of edge directions, even without precise knowledge of the corresponding gradient or edge positions. This idea is exploited by the Histogram of Oriented Gradients (HOG) descriptors [52]. They use a dense representation of the image by means of a local statistic of edge orientations. The image is divided into small regions called cells and for each cell a histogram of the gradient orientations over the pixels is calculated. The combination of the histograms of the different cells provides the image representation. In constructing the histogram, the gradient orientations are weighted by their magnitude, in order to promote the contribution of pixels located on the edges. The contribution of each pixel is distributed into adjacent cells using a Gaussian weighting window in order to prevent boundary effects. Normalization over group of cells, followed by clipping, is frequently used for reducing the effects of non-linear illumination changes. For MARFE images this step can be skipped because plasma events (MARFE and non-MARFE) appear mainly as bright features on a dark background, with a low contrast variation along the image stream. The HOG descriptors are usually associated with a recognition system based on supervised learning. Support Vector Machines (SVM) classifiers [53], which are based on the concept of decision planes that define decision boundaries, represent an efficient and reliable choice.

HOG descriptors provide a dense and robust coding of shapes ensuring strong discrimination power. However the processing time for evaluating the descriptors represents a critical issue. Possible solutions for this problem are the integration of a cascade-of-rejecters and the use of AdaBoost to train the chain of rejection rules [54], or the parallel implementation using the GPGPU (General Purpose computation on Graphics Processing Units) technology [55-56]. The last approach has been recently applied for MARFE automatic identification [51]. The implementation uses a region of interest which encompasses the area where most of the MARFEs in the JET database leave a signature, in order to diminish the computation time for gradients evaluation. On the other hand the latency of CPU global memory access can be minimized by copying a large amount of data in the GPU memory and allowing a large number of active threads. Therefore a set of consecutive frames are grouped in a “combined image” which is copied and processed into the GPU memory. The computation time needed for an image is ~0.65ms, which is approximately twenty times greater than the time interval between consecutive frames (the frame rate of the KL-8 fast visible camera

is ~0.33 ms). Obviously it is not possible analyze all the images in the stream. Therefore a criterion to select the images susceptible to contain MARFE events has been defined. It is based on the sum of grey-levels in the image, reflecting the idea that both MARFE and non-MARFE events produce images with enhanced brightness. The HOG calculations are started only if this criterion is satisfied. The contiguous sequence of frames for which the HOG computation is launched define an interval of interest (IOI) - see Fig. 7. The gap between consecutive IOIs can be smaller than the dimension of a "combined image". This means that immediately after the analysis of an IOI, another one should be processed, delaying the response of the classifier. The average value of the time needed for prediction, calculated for the whole JET database, is ~15.4 ms while the maximum delay is ~42 ms. As the time difference between the MARFE occurrence and the following disruption is usually of the order of several hundreds of milliseconds, the HOG method is able to provide the prediction fast enough to allow sufficient time for the intervention of mitigation tools, in order to reduce the detrimental effects of disruptions. The classifier reached a success rate of 100%, even if only 77.8% images displaying MARFE shapes have been identified. The reasons for this difference may be the use of the region of interest which captures only a part of the MARFE signatures and also the selection of frames for building the training set.

A significant effort has been spent in developing methods suitable for automatic MARFE detection because they may provide new information potentially useful for disruption prediction. However the methods developed address also the identification of other harmful events. For example the detection of UFOs may provide useful information for preventing significant damages to the plasma facing components. UFOs appear in video images as bright small particles moving fast inside the vessel. The spatial resolution of the camera does not allow the disclosure of many details of their shape. Therefore distinguishing UFOs from hot spots (static regions of the vacuum vessel reaching high temperatures due to concentrated plasma-wall interactions) may be achieved capturing information about their dynamic. The pixels with variation in intensity are identified by using a high pass filter for extracting the high frequency components of the image. As the filter parameters may vary with the image characteristics, a pragmatic procedure consists of subtracting a blurred version of the image from the original one has been used. The resulting frame is scanned by an edge detector algorithm. The Laplacean filter proved to give the best trade-off between results and computational costs. Spurious discontinuities may result after edge detection. Therefore edge linking algorithms, based on simple morphological operators (dilation, erosion) have to be used to group edge pixels into meaningful edges. The last step consists of the discrimination of UFOs based on the dynamic criteria (mainly the changing rate of shape and position). The dynamic analysis of UFOs is particularly difficult because a high number of objects have to be followed on complex trajectories which can intersect and can be occluded by structures or simply present discontinuities due to changes in emission. First encouraging results have reported [37] but these extremely complex procedures are still subject of further development.

## 4. IMAGE PROCESSING FOR LONG TERM TRENDS ASSESSMENT

The useful video information related to several physical phenomena (instabilities, pellets, filaments) and to events detection can be retrieved, after complex processing procedures, from a limited number of frames or at most from the whole set of images corresponding to a JET pulse. However, in case of other phenomena, the meaningful information is unveiled only after a large number of experiments or after a whole experimental campaign.

For example, the interaction between the tiles and dust or droplets mobilized during the discharges lead to the formation of spots appearing in the images provided by the KL-9B infra-red (IR) camera system. This camera is installed on the top of JET vacuum vessel (Fig.8), viewing the JET divertor from the top of the machine. It operates between 3.5-5mm and up to sampling frequencies of ~20kHz [57]. The evolution of the spots properties (such as size and distribution) and their correlation with macroscopic events become available only after scrutinizing of a long series of experiments. Obviously, for the assessment of long term trends, which imply the processing of a large amount of videos, automatic image processing tools are essentials. These tools have to be tailored to take into account the specificities of the images recorded by the camera. The KL-9B camera delivers images with wide varying brightness. For a certain range of brightness, spots with variable intensities, irregular shapes and lying on a variable background become visible (see again Fig.8). Sudden changes of the brightness may arise due to the occurrence of plasma instabilities which produce light signals (such as e.g. ELMs).

Several notorious spot detection methods have been tested, but the experiments revealed difficulties in customizing these methods for the specific problem of spot detection and characterization in images recorded by the KL-9B camera. Due to the background non-uniformity the watershed method [58] provides over-segmentation. The variability of images and spot properties imposes the readjustment of several parameters in case of the active contours methods [59], with negative effects for automating the image processing chain. It has also to be mentioned that the use of morphological operators using specific structuring elements is prone to altering the shapes of the spots, causing difficulties in the interpretation of the results. Therefore a specific semi-empirical technique has been developed. It does not use any prior assumption regarding the spots parameters and distribution, allowing the preservation of the irregular shapes.

The first step of this method consists of the determination of local intensity maxima by using the MAX-MIN filter [60]. This method allows an efficient implementation which provides robust results reducing in the same time the computer latency and memory usage. Then a circular search is performed around each local maximum. The ratio between the intensity of the local maximum and the average intensity of the neighbouring pixels should exceed a pre-defined limit (the same for all images), preventing the classification of flat regions as spots. In agreement with the experimental observations, the size of the spots is limited by checking if, at a certain distance from the local maximum (the same distance has been used for all analysed images), the pixels intensities fall below a certain threshold. This threshold depends on the image average grey-level and therefore it has to be determined empirically. Its value has been adjusted manually for a set of images with

average grey-level covering the whole range observed experimentally, in order to obtaining a 'good' spot detection. The quality of the spot identification has been judged by visual inspection. A linear dependence of the threshold value with respect to the average grey-value has been obtained and used in the automatic analysis of all videos. An illustration of the quality of spots detection is presented in Fig.9. The details of the algorithm briefly described here can be found in Ref. 61 together with additional results.

Spots identification in a set of videos is followed by the determination of different spots parameters: the evolution of the area covering the divertor tiles, the size distribution, identification and labelling of frames containing giant spots, etc. For example, the evolution of the total spot area covered by spots for the divertor tiles is illustrated in Fig.10.

During the experiments, characteristic patterns are evolving with significant changes occurring at relatively long intervals of time. For assessing this evolution the correlation coefficient is calculated for each pair of successive spot patterns:

$$corr = \frac{N^2 \Sigma_i f_i^k f_i^{k-1} - \Sigma_i f_i^k \Sigma_i f_i^{k-1}}{[N^2 \Sigma_i (f_i^k)^2 - (\Sigma_i f_i^k)^2]^{1/2} [N^2 \Sigma_i (f_i^{k-1})^2 - (\Sigma_i f_i^{k-1})^2]^{1/2}} \quad (11)$$

where is the total number of pixels in the image and and are the indexes of the current pair of images - this coefficient has the value 1 for identical images. Its evolution displays several peaks, corresponding to regions where a high correlation between patterns exists (Fig.10). For the sequence of pulses where the pattern remains approximately unchanged, a general characteristic configuration can be obtained by merging all patterns in one image and applying an appropriate threshold.

Spot pattern clusterization is useful for determining the correlation with macroscopic events. The transition between successive kinds of spot patterns has been found to correlate with pulse intervals characterized by a series of intentional disruptions and related studies (such as massive gas injection). This is illustrated also in Fig.10, which relates the main variations in the correlation coefficient with the main features of the corresponding experimental programme. This analysis has been performed on a set of 190 videos from the data existent for JET Pulse No's: range 80380-83165. The data selection and retrieval has been facilitated by the software platform PINUP (*Plasma ImagiNg data Understanding Platform*) [62-63], developed for imaging diagnostics data and integrated into the JET data computing environment.

Further systematic surveys are to be undertaken in the future JET campaigns in order to obtain new insights related to the evolution of spots properties and their relation with macroscopic events.

## CONCLUSIONS

Image processing tools are already common instruments in plasma diagnostics on JET and it can be forecasted that they will become indispensable for the safe operation of the next generation of fusion devices and for maximizing the scientific exploitation. Besides the tools developed for the active protection of the plasma facing components, which are routinely used during JET experiments and besides the intelligent and automatic techniques for handling and data mining the growing

database, the image processing, analysis and interpretation for extracting physical information has also reached maturity. Working in an imagistic environment usually characterized by significant noise, saturation and various artefacts and populated by a wide typology of objects, these methods achieved several noteworthy results. The optical flow techniques proved to be a reliable tool for evaluating the ice extrusion velocity in the process of pellet injection (with real-time capabilities) and also for deriving information related to pellet cloud dynamic and drifts. A package of methods has been developed for automatic events detection. Several classifiers developed for retrieving MARFEs signature in video data are compatible with on-line implementation and allow a good rate of correct classification and a low rate of false alarms. As MARFEs normally precede disruptions in density limit discharges, these methods represent a first image based approach for disruption prediction. An effective implementation depends on the future upgrade of the hardware of the cameras in order to allow real time data streaming. The interaction between the divertor tiles and the dust mobilized during the discharges has been addressed by developing tools for detection and analysis of the spots subsequently occurring in IR images. The assessment of the long term trends in their evolution makes possible the correlation with macroscopic events. As future nuclear devices will be equipped with a significantly increased number of high performance imaging systems, it is expected that image processing methods for extracting physical information will face new challenges in what concerns the detection, analysis and interpretation of physical phenomena leaving signatures in the video data, simultaneously with the necessity to be able to manage massive data production and real time requirements.

**ACKNOWLEDGMENT**

This work was supported by the European Communities under the contract of Association between EURATOM and MEdC and ENEA was carried out within the framework of the European Fusion Development Agreement. The views and opinions expressed herein do not necessarily reflect those of the European Commission.

**REFERENCES**

[1]. G.F. Matthews, M. Beurskens, S. Brezinsek, M. Groth, E. Joffrin, A. Loving, M. Kear, M-L. Mayoral, R. Neu, P. Prior, V. Riccardo, F. Rimini, M. Rubel, G. Sips, E. Villedieu, P. de Vries, M.L. Watkins, JET ITER-Like Wall - Overview and Experimental Programme, Physica Scripta **T145**(2011)014001.

[2]. A. Huber, S. Brezinsek, Ph. Mertens, B. Schweer, G. Sergienko, A. Terra, G. Arnoux, N. Balshaw, M. Clever, T. Edlingdon, S. Egner, J. Farthing, M. Hartl, L. Horton, D. Kampf, J. Klammer, H.T. Lambertz, G.F. Matthews, C. Morlock, A. Murari, M. Reindl, V. Riccardo, U. Samm, S. Sanders, M. Stamp, J. Williams, K.D. Zastrow, C. Zauner, A new Radiation-Hard Endoscope for Divertor Spectroscopy on JET, Fusion Engineering and Design, Article in press., DOI: 10.1016/j.fusengdes.2013.02.053.

[3]. M. Clever, G. Arnoux, N. Balshaw, P. Garcia-Sanchez, K. Patel, G. Sergienko, D. Soler, M.F.

Stamp, J. Williams, K.-D. Zastrow, A wide angle view imaging diagnostic with all reflective, in-vessel optics at JET, Fusion Engineering and Design, Article in press., DOI: 10.1016/j.fusengdes.2013.01.038.

[4]. I.Balboa, G. Arnoux, T. Eich, B. Sieglin, S. Devaux, W. Zeidner, C. Morlock, U. Kruezi, G. Sergienko, D. Kinna, P.D. Thomas, M. Rack, Upgrade of the infrared camera diagnostics for the JET ITER-like wall divertor, Review of Scientific Instruments, **83-10**(2012)10D530.

[5]. S. Devaux, G. Arnoux, Y. Corre, J-L. Gardarein, J. Gaspar, P. Jacquet, F. Marcotte, G. Matthews, P. Beaumont, S. Cramp, S. Dalley, D. Kinna, A. Horton, P. Lomas, Ph. Mertens, V. Riccardo, D. Valcàrcel, Calorimetry of the JET ITER-Like Wall components, Journal of Nuclear Materials, 2013, Article in Press.

[6]. G. Arnoux, T. Farley, C. Silva, S. Devaux, M. Firdaouss, D. Frigione, R.J. Goldston, J. Gunn, J.Horacek, S. Jachmich, P.J. Lomas, S. Marsen, G.F. Matthews, R.A. Pitts, M. Stamp, P.C. Stangeby, Scrape-off layer properties of ITER-like limiter start-up plasmas in JET, (2013) Nuclear Fusion, **53** (7), art. no. 073016.

[7]. M. Lehnen, G. Arnoux, N. Baumgarten, S. Brezinsek, S. Devaux, A. Huber, S. Jachmich, U. Kruezi1, G.F. Matthews, C. Reux, V. Riccardo, B. Sieglin, M.F. Stamp, P.C. de Vries, Disruption heat loads and their mitigation in JET with the ITER-like wall, Journal of Nuclear Materials, 2013, Article in press.

[8]. S. Palazzo, A. Murari, G. Vagliasindi, P. Arena, D. Mazon, A. De Maack, Image processing with cellular nonlinear networks implemented on field-programmable gate arrays for real-time applications in nuclear fusion, Review of Scientific Instruments **81** (2010)083505.

[9]. J. Vega, A. Murari, A. Pereira, A. Portas, R. Castro, Review of Scientific Instruments, Intelligent technique to search for patterns within images in massive databases, 79–10 (2008) 10F327.

[10]. J. Vega, A. Murari, A. Pereira, A. Portas, G.A. Ratta, R. Castro, Overview of intelligent data retrieval methods for waveforms and images in massive fusion databases, Fus. Eng. Des.84 (2009) 1916.

[11]. J.Vega,A.Murari,S.González, A universal support vector machines based method for automatic event location in waveforms and video-movies: Applications to massive nuclear fusion databases, Review of Scientific Instruments **81** (2010)023505.

[12]. B. Jähne, Digital Image Processing, 6th ed. 2005, Springer, 2005.

[13]. B. Horn, B. Schunck, Determining optical flow. Artificial Intelligence, 17(1981)185–203.

[14]. B. Lucas, T. Kanade, "An iterative image registration technique with an application to stereo vision". In Proc. Seventh International Joint Conference on Artificial Intelligence, Vancouver, Canada, 1981, pp. 674–679.

[15]. S. Baker, D. Scharstein, J.P. Lewis, S. Roth, M.J. Black, R. Szeliski, A database and evaluation methodology for optical flow, Int. J. Comput. Vision 92 (2011) 1.

[16]. A. Bruhn, J. Weickert, C. Schnorr, Lucas/Kanade meets Horn/Schunck: combining local and global optic flow methods, International Journal of Computer Vision, **61-3**(2005)211-231.

[17]. T. Craciunescu, A. Murari, A. Alonso, P.T. Lang, G. Kocsis, I. Tiseanu, V. Zoita., "Application of Optical Flow Method for Imaging Diagnostic in JET", ournal of Nuclear Materials, **400-**

3(2010)205-212.
[18]. Alonso, P. Andrew, A. Neto, J. L. de Pablos, E. de la Cal, H. Fernandes, J. Gafert, P. Heesterman, C. Hidalgo, G. Kocsis, A. Manzanares, A. Murari, G. Petravich, L. Rios, C. Silva, P.D. Thomas, Fast visible camera installation and operation in JET, International Conference on Burning Plasma Diagnostics, Varenna, Italy, 24–28 Sept. 2007, AIP Conf. Proc. 988, pp. 185-188.
[19]. E. Gauthier, H. Roche, E. Thomas, S. Droineau, B. Bertrand, J.B. Migozzi, W. Vliegenthart, L. Dague, P. Andrew, T. Tiscornia, D. Sands, ITER-like wide-angle infrared thermography and visible observation diagnostic using reflective optics, Fusion Engineering and Design, **82**- 5–14(2007) 1335-1340.
[20]. E. Mémin, P. Pérez, Dense estimation and object-based segmentation of the optical flow with robust techniques. IEEE Transactions on Image Processing, **7-5**(1998)703–719.
[21]. L. Alvarez, R. Deriche, T. Papadopoulo, J. Sanchez, Symmetrical dense optical flow estimation with occlusion detection, In ECCV, pages 721.735, 2002.
[22]. S. Roth, V. Lempitsky, C. Rother, Discrete-Continuous Optimization for Optical Flow Estimation, D. Cremers et al. (Eds.): Visual Motion Analysis, LNCS 5604, pp. 1–22, Springer-Verlag Berlin Heidelberg 2009.
[23]. W. Fundamenski, R.A. Pitts, G. Arnoux, M. Jakubowski, A. Loarte, M. Beurskens, ELM Filament Heat Loads on Plasma Facing Components in JET and ITER, Proceedings of the 22nd IAEA Fusion Energy Conference, Geneva, Switzerland.
[24]. B. Lipschultz, B. Labombard, E.S. Marmar, M.M. Pickrell, J.L. Terry, R. Watterson And S.M. Wolfe, MARFE: An Edge Plasma Phenomenon, Nuclear Fusion, vol. **24-8**(1984) 977-988.
[25]. S.L. Milora, W.A. Houlberg, L.L. Lengyel and V. Mertens, Pellet fuelling, Nuclear Fusion **35** (1995) 657.
[26]. P.T. Lang, H. Zohm, K. Buchl, J.C. Fuchs, O. Gehre, O. Gruber, V. Mertens, H.W. Muller and J. Neuhauser, Pellet fuelling of ELMy H mode discharges on ASDEX Upgrade, Nuclear Fusion **36** (1996) 1531.
[27]. P.T. Lang, P. Cierpka, J. Harhausen, M. Kaufmann, J. Neuhauser, C. Wittmann, ASDEX Upgrade Team, G. Kocsis, J. Sárközi, T. Szepesi, C. Dorner, G. Kauke, pellet launcher tool optimized for the control of edge localized modes in ASDEX Upgrade H-mode plasmas, Fusion Engineering and Design **82** (2007) 1073-1080.
[28]. G. Kocsis, L. Barrera, J.E. Boom, T. Craciunescu, G. Cseh, P.T. Lang, N.C. Luhmann Jr., G. Náfrádi, H.K. Park, T. Szepesi, Investigating pellet ablation dynamics at ASDEX Upgrade, Conference on Plasma Phys. Sofia, June 29 - July 3, 2009 ECA Vol.33E, P-1.151 (2009)
[29]. G. Kocsis, S. Kalvin, G. Veres, P. Cierpka, P.P.T. Lang, J. Neuhauser, C. Wittman, C, fast framing camera system for observation of acceleration and ablation of cryogenic hydrogen pellet in ASDEX Upgrade plasmas, Review of Scientific Instruments **75**(2004) 4754 – 4762.
[30]. A. Géraud, M. Lennholm, T. Alarcon, P. Bennett, D. Frigione, D. Garnier, P.T. Lang, A. Lukin, R. Mooney, I. Vinyar, Status of the JET high frequency pellet injector, Fusion Engineering and Design, 2013, Article in Press, DOI: 10.1016/j.fusengdes.2012.12.019
[31]. T. Craciunescu, P. Lang , A. Murari, T. Szepesi, S. Kálvin., G. Kocsis, A. Alonso, I. Tiseanu,

V. Zoita. Determination of the pellet parameters by image processing methods, Fusion Engineering and Design, 86(2011)1186-1190.

[32]. ISO/IEC CD 13818-2. ITU-T H.262 (MPEG-2 Video), Information technology. Generic coding of moving pictures and associated audio information: Video, 1995.

[33]. M.T. Coimbra, M. Davies, IEEE Trans. Circuit Syst. Video Tech. **15** (2005) 103.

[34]. B. Shen, K. Sethi, Proc. SPIE Storage Retrieval Image Video Databases IV 2670 (1996) 404.

[35]. R.H. Chung, F.Y. Chin, K.Y. Wong, K.P. Chow, T. Luo, H.S. Fung, Efficient block- based motion segmentation method using motion vector consistency, in: Proceedings of the IAPR Conference on Machine Vision Applications MVA- 2005, May 16–18, 2005, Tsukuba Science City, Japan, pp. 550–553.

[36]. T. Craciunescu, A. Murari, P.T. Lang, I. Tiseanu, Motion Estimation Within the MPEG Video Compressed Domain for JET Plasma Diagnostics, Nuclear Instruments and Methods in Physics Research Section A, **659-1**(2011)467.

[37]. A. Murari, M. Camplani, B. Cannas, D. Mazon, F. Delaunay, P. Usai, And J. Delmond, Algorithms for the automatic identification of MARFEs and UFOs in JET database of visible camera videos, IEEE Trans. On Plasma Science, **38-12**(2010)3409–3418.

[38]. N. McFarlane and C. Schofield, Segmentation and tracking of piglets in images, Machine Vision and Applications **8**(3), pp. 187–193, 1995.

[39]. M. K. Hu, Visual Pattern Recognition by Moment Invariants, IEEE Transactions on Information Theory, IT-8(1962)179–187.

[40]. M. Portes de Albuquerque, A. Murari, M. Giovani, N. Alves Jr., Marcelo P. de Albuquerque, A 10,000 images per second parallel algorithm for real time detection of MARFEs on JET, IEEE Transactions on Plasma Science, 41-2(2013)341-349.

[41]. M.C. Morrone, R.A. Owens, Feature Detection from Local Energy, Pattern Recognition Letters, **6-5**(1987)303-313.

[42]. P. Kövesi, Image features from phase congruency, VIDERE: International Journal of Computer Vision, vol. **1**, no. 3, pp. 1-26, 1999.

[43]. Hans G. Feichtinger, Thomas Strohmer: "Gabor Analysis and Algorithms", Birkhäuser, 1998.

[44]. G. Daugman, An information–theoretic view of analogue representation in striate cortex, Computational Neuroscience, Ed. Schwartz, E.L., Cambridge, MA: MIT Press, **403–424**, 1990.

[45] Z. Wang, A.C. Bovik, H.R. Sheikh, And E. P. Simoncelli, Image quality assessment: From error visibility to structural similarity,IEEE Transactions on Image Processing, **13-4**(2004)600–612.

[46]. T. Craciunescu, A. Murari, I. Tiseanu, J. Vega, Phase Congruency Image Classification for MARFE Detection on JET with a Carbon Wall, Fusion Science and Technology, **62**-2(2012)339-346.

[47]. M. Elad, M. Aharon, Image Denoising Via Sparse and Redundant Representations Over Learned Dictionaries, IEEE Transactions on Image Processing, **15**-12(2006)3736-3745.

[48]. J. Mairal, F, Bach, J. Ponce, G. Sapiro, A. Zisserman, Discriminative learned dictionaries for local image analysis, Proc. of the IEEE Conference on Computer Vision and Pattern

Recognition, 23-28 June 2008, Anchorage, USA, pp. 1-8.
[49]. M. Aharon, M., Elad, A., Bruckstein, K-SVD: An algorithm for designing overcomplete dictionaries for sparse representation, IEEE Transactions on Signal Processing, **54**-11(2006) 4311-4322.
[50]. G. Davis, S. Mallat, and M. Avellaneda, Adaptive greedy approximations, J. Construct. Approx., vol. **13**, pp. 57–98, 1997.
[51]. T. Craciunescu, A. Murari, I. Tiseanu, J. Vega, Supervised Image Processing Learning for MARFE Detection JET with a Carbon Wall, to be submitted to IEEE Trans. Plasma Science.
[52]. N. Dalal, B. Triggs, Histograms of Oriented Gradients for Human Detection, International Conference on Computer Vision & Pattern Recognition (CVPR '05) 1 (2005) 886-893.
[53]. V.N. Vapnik, The Nature of Statistical Learning Theory, Springer-Verlag, 1995.
[54]. Q. Zhu, M.C. Yeh, K.T. Cheng ; S. Avidan, Fast Human Detection Using a Cascade of Histograms of Oriented Gradients, IEEE Computer Society Conference on Computer Vision and Pattern Recognition (CVPR) 17-22 June 2006, New York, NY, USA, p. 1491 – 1498.
[55]. V.A. Prisacariu, I.D. Reid, fastHOG - a real-time GPU implementation of HOG, http://www.robots.ox.ac.uk/~lav/Papers/prisacariu_reid_tr2310_09/prisacariu_reid_tr2310_09.html, 2009.
[56] Y.P. Chen, S.Z. Li, X.M. LIN, Fast HOF Feature Computation based on CUDA, 2011 IEEE International Conference on Computer Science and Automation Engineering (CSAE), 1-12 June 2011, Shanghai, China, p. 748-751.
[57]. I.Balboa, G. Arnoux, T. Eich, B. Sieglin, S. Devaux, W. Zeidner, C. Morlock, U. Kruezi, G. Sergienko, D. Kinna, P.D. Thomas, M. Rack, Upgrade of the infrared camera diagnostics for the JET ITER-like wall divertor, Review of Scientific Instruments, **83**-10(2012)10D530.
[58]. S. Beucher, C. Lantuéjoul, Use of watersheds in contour detection, In International workshop on image processing, real-time edge and motion detection. http://cmm.ensmp.fr/~beucher/publi/watershed.pdf.
[59]. T.F. Chan and L.A. Vese, Active Contour Without Edges, IEEE Transactions on Image Processing, **10**-2(2001)226-277.
[60]. D. Lemire, Streaming Maximum-Minimum Filter Using no more than Three Comparisons per Element, Nordic Journal of Computing, Volume **13**-4(2006)328-339.
[61]. T. Craciunescu, A. Murari, B. Sieglin, G. Matthews, An Original Spot Detection Method for Large Surveys of Videos in JET, preprint SM-PR(13)27, submitted to IEEE Transactions on plasma science : SM-PR(13)27
[62]. V. Martin, V. Moncada, G. Dunand, Y. Corre, E. Delchambre, J.M. Travere, Integrated software for imaging data analysis applied to edge plasma physic and operational safety", Fusion Engineering and Design, **86**-4(2010)270-278.
[63]. V. Martin, V. Gervaise, V. moncada, J.M. Travere, M.H. Aumeunier, M. Firdaouss, M. Houdeau, T. Loarer, S. Devaux, G. Arnoux, D. Kinna, "A New Integrated Software Platform for the Analysis of JET ITER-like Wall Imaging Diagnostics Data", Proc. of 27th Symposium on Fusion Technology, Sept. 24-28, 2012, Liege, Belgium (to be published in Fusion Engineering and Design).

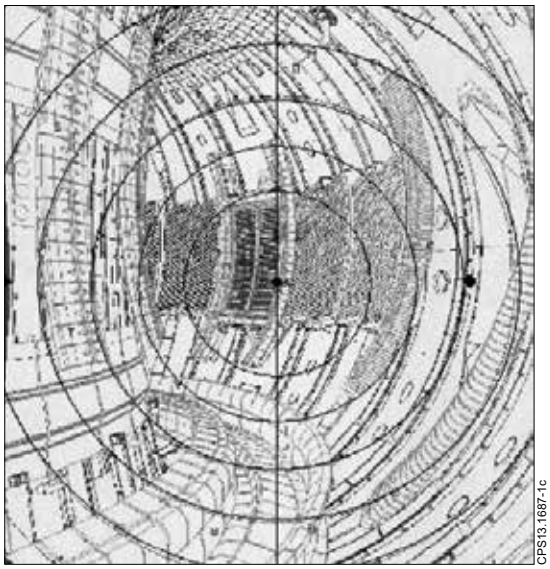


*Figure 1: The field of view of the fast visible camera.*

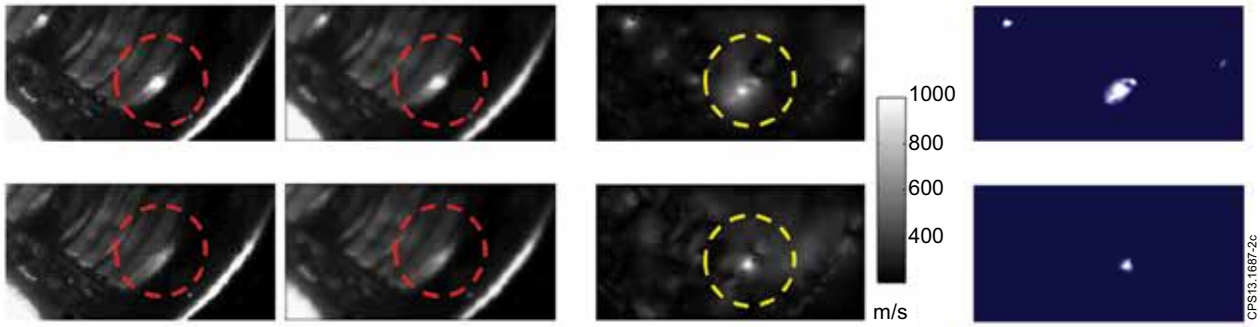


*Figure 2:ELM filaments moving up along the poloidal limiters (left - consecutive video frames are shown in each row), the calculated modulus of the optical flow field (middle) and motion segmentation (right). The moving filaments and are marked by red dashed circles while the corresponding optical flow is marked by yellow dashed circles. Images are recorded for JET Pulse No: 69903.*

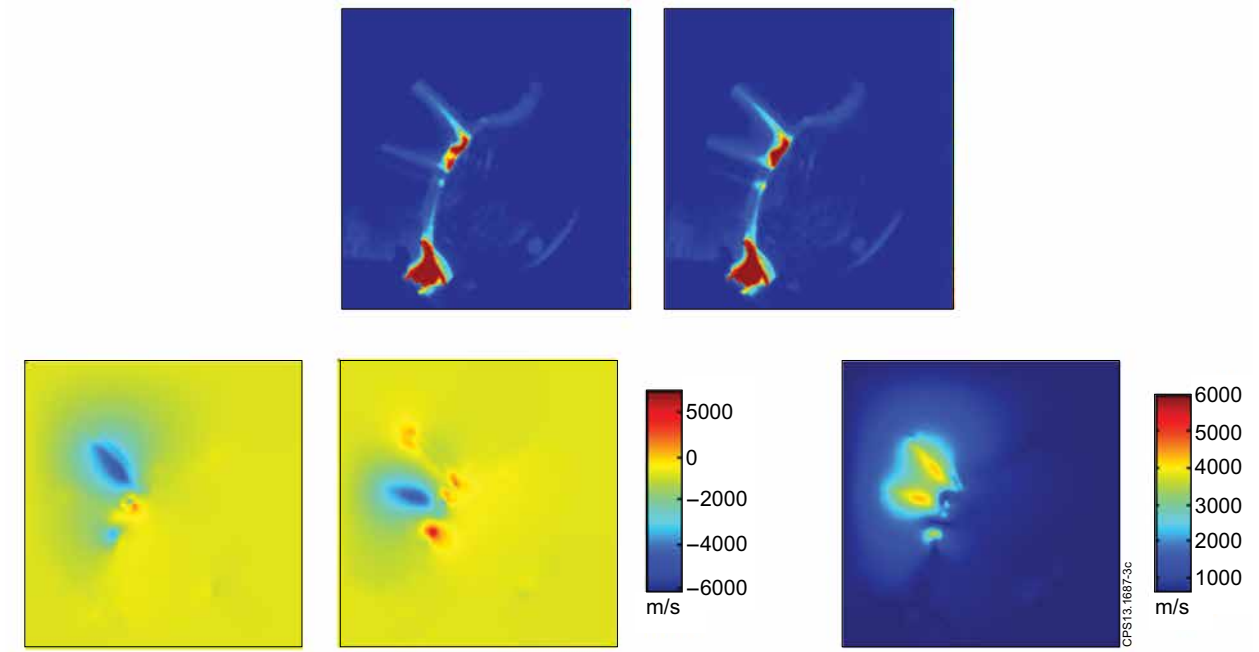


*Figure 3: Illustration of the optical flow calculation for MARFE: consecutive video frames (top), horizontal component (bottom left), vertical component (bottom middle) and modulus (bottom right).*

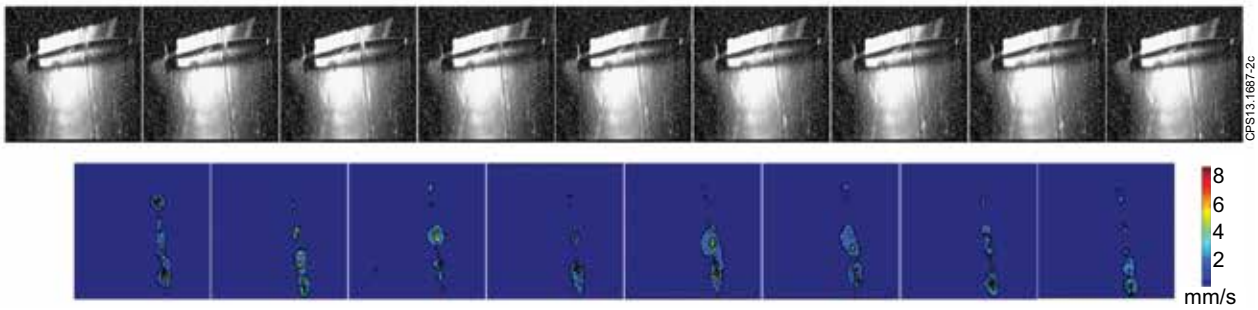


*Figure 4: A sequence of frames from the video showing the extruded deuterium ice in case of JET Pulse No: 76379 (top) and the corresponding optical flow evaluation (bottom). Due to strong saturation of the images provided by the video camera, the ice ribbon-structure is only partially visible. Therefore the speed velocity field is reconstructed only when the visible ribbon structure is clearly identified.*

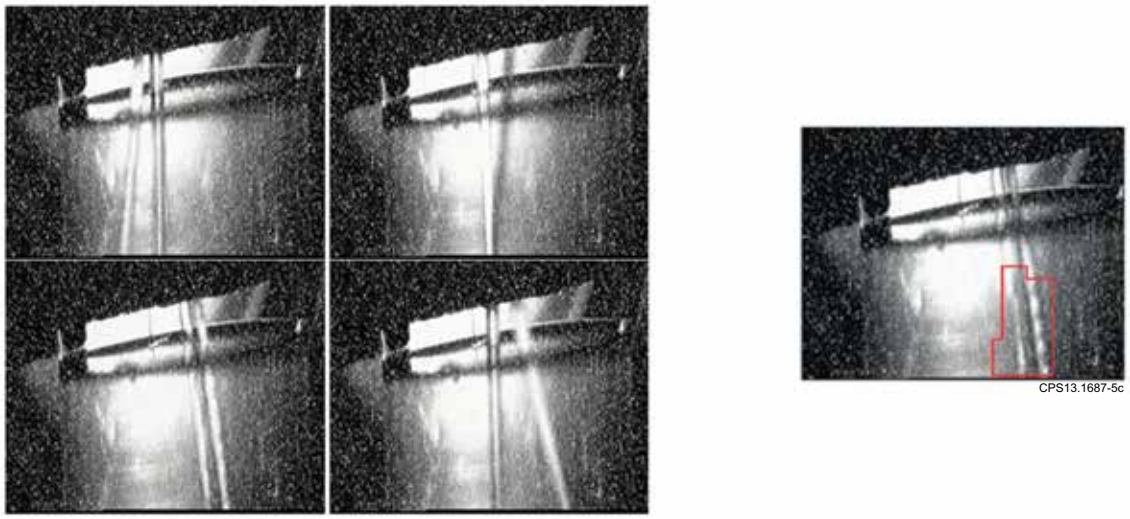


*Figure 5: The ribbons of ice floating during the extrusion process (left). The motion segmentation provided by the MPEG motion vectors is represented by the red perimeters (right).*

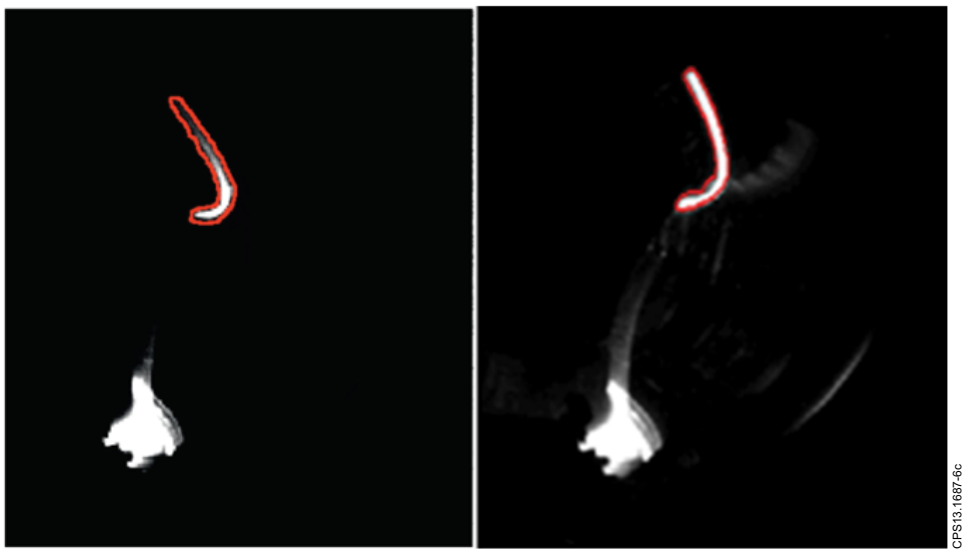


*Figure 6: Example of detected MARFE by background subtraction [38](left) and by processing the MPEG motion field [36] (right).*

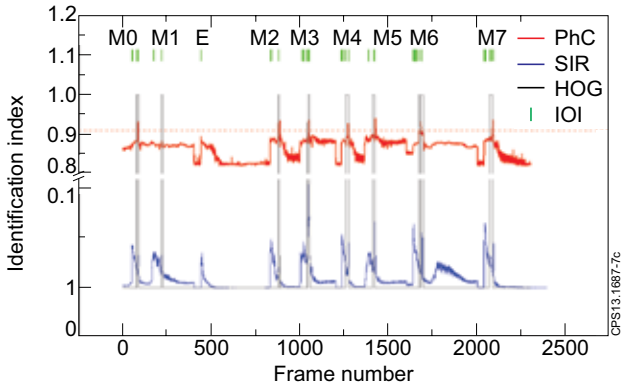


*Figure 7: The evolution of the identification index for PhC, SR and HOG classifiers in case of the JET Pulse No: 50053. During this discharge a number of 7 MARFE events occurred (M1, …, M7). PhC succeeds to identify all MARFE events except M1, for which the (red curve) is below the threshold level (dot red curve). The blue curve shows the evolution of the similarity index in case of SIR. With one exception (the misclassified event E) the narrow peaks correspond to MARFE events. HOG identify correctly all the MARFE events without generating misclassified events – the grey curve depicts the output of the trained SVM (grey curve) and the green bars mark the frames for which the HOG calculation is launched.*

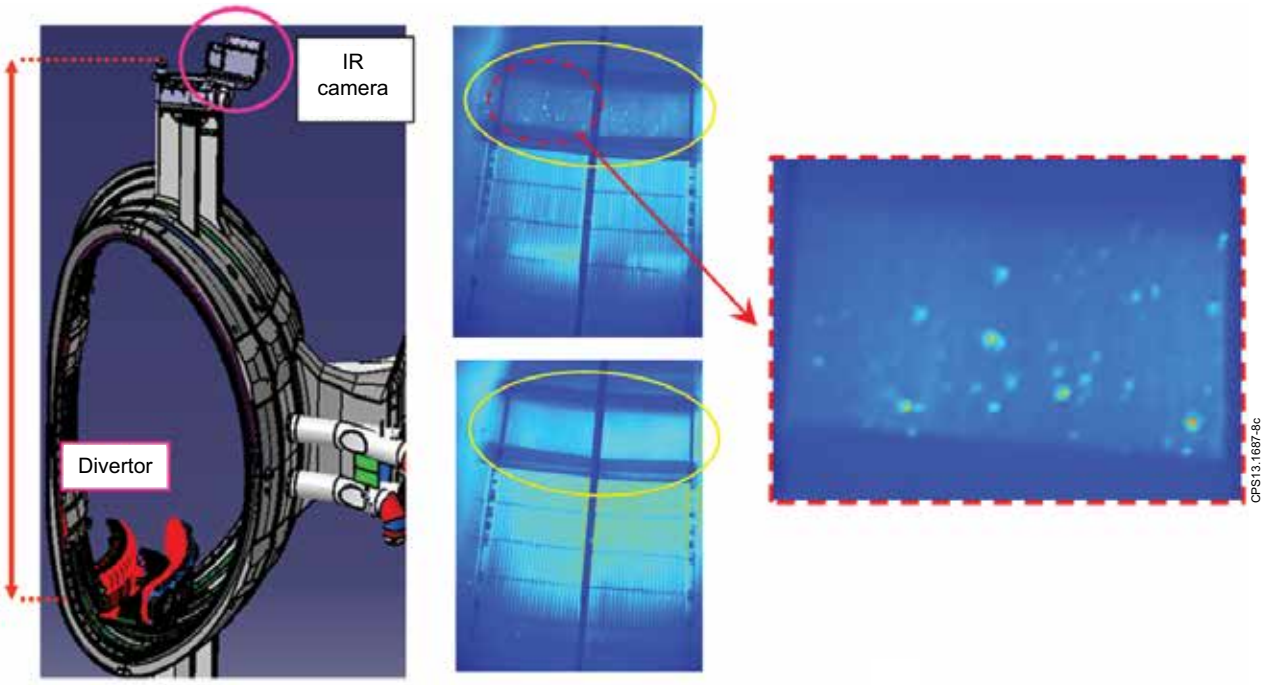


*Figure 8: Illustration of the location of the IR camera (left) and typical images recorded revealing spots with variable intensities and lying on a variable background (middle). The region corresponding to the two tiles of the divertor is marked by the yellow contour. A zoom of the region corresponding to the left tile make visible the irregular shapes of the spots (right).*

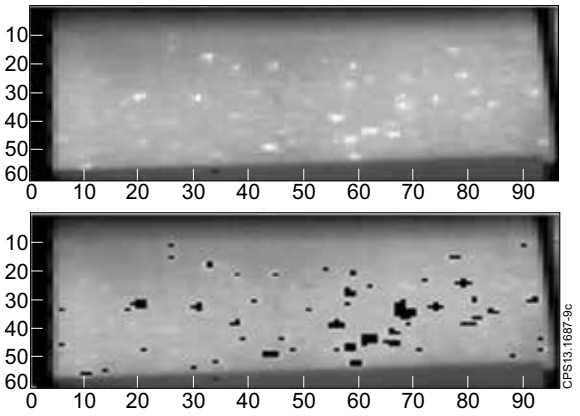


*FIgure 9: Illustration of the quality of the automatic procedure for automatic spot detection - the original frame no. 1043 from the video corresponding to the JET Pulse No: 81423 (top) and the same frame with detected spots superimposed as black areas (bottom).*

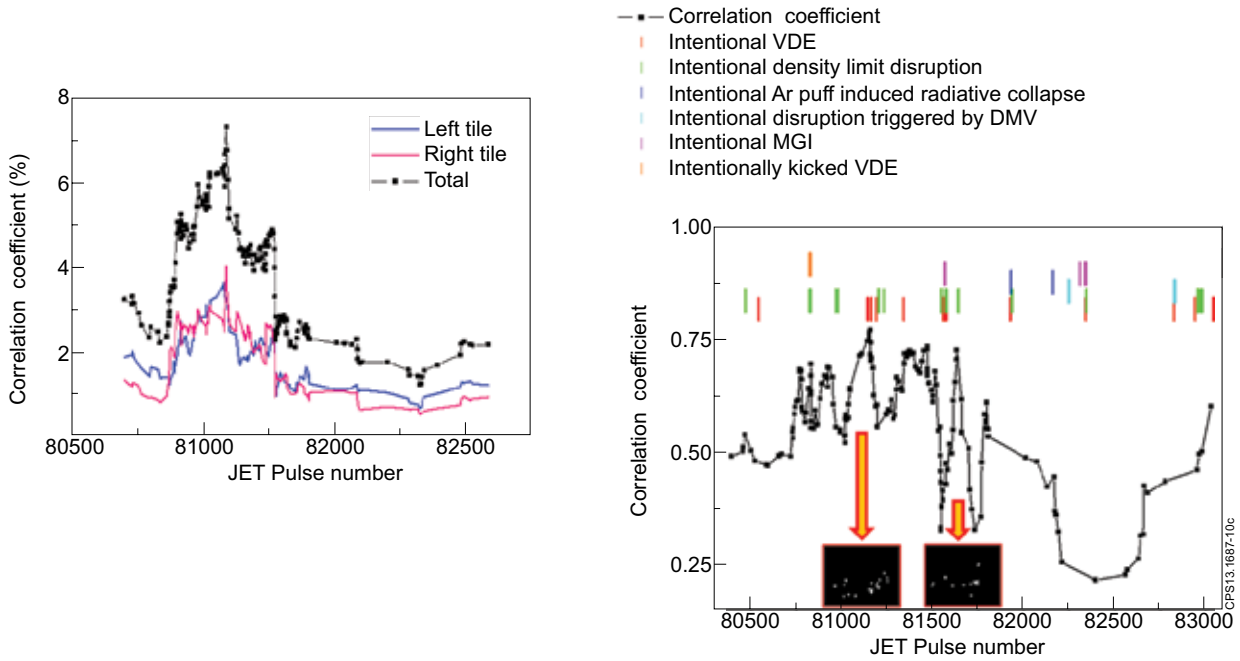


*Figure 10: Illustration of the results retrieved from the spot detection and analysis: the evolution of the spot area covering the divertor tiles (left); the evolution of the correlation coefficient between successive spot patterns and relation between the abrupt reductions in the correlation coefficient value and the experiments, mainly related to intentional disruptions - VDR: Vertical Displacement Events DMV: Diagnostic Mass Valve MGI: Massive Gas Injection; two typical general configuration of spots characterizing a sequence of pulses depicted as inserts (right).*